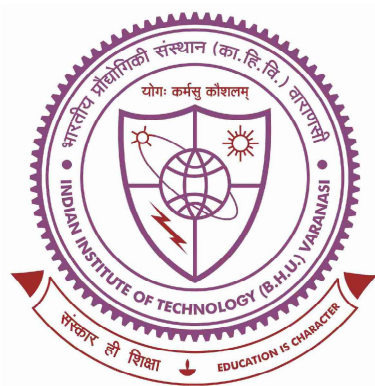


**Study of evolution of energetically favored collectivity and hindered isomeric states in the  $A \approx 90$  region**



**Thesis submitted in partial fulfillment  
for the Award of  
DOCTOR OF PHILOSOPHY  
in  
PHYSICS**

*by*  
**NIDHI GOEL**

*Under the supervision of*  
**Dr. Somnath Nag**

**DEPARTMENT OF PHYSICS  
INDIAN INSTITUTE OF TECHNOLOGY  
BANARAS HINDU UNIVERSITY  
VARANASI - 221005**

**ROLL NUMBER**  
18171505

**YEAR OF SUBMISSION**  
2024

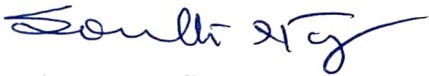


I would like to dedicate this thesis to my loving parents, my supportive husband and amazing friends, whose support and motivation kept me going through the tough times.



## Certificate

It is certified that the work contained in the thesis titled "*Study of evolution of energetically favored collectivity and hindered isomeric states in the  $A \approx 90$  region*" by *Ms. Nidhi Goel*, Roll Number **18171505**, has been carried out under my supervision, and this work has not been submitted elsewhere for a degree.



**Signature:**

**Supervisor**

Dr. Somnath Nag

(Assistant Professor)

Department of Physics

Indian Institute of Technology (BHU),

Varanasi-221005 (U.P.), India

**Assistant Professor**

**Department of Physics**

**Indian Institute of Technology**

**(Banaras Hindu University)**

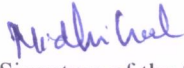
**Varanasi-221005**



## Declaration

I, **Nidhi Goel**, certify that the work embodied in this thesis is my own bona-fide work and carried out by me under the supervision of **Dr. Somnath Nag** from January 2019 to December 2024 at the **Department of Physics**, Indian Institute of Technology (BHU), Varanasi. The matter embodied in this thesis has not been submitted for the award of any other degree/diploma. I declare that I have faithfully acknowledged and given credits to the research workers whenever and wherever their works have been cited in my work in this thesis. I further declare that I have not wilfully copied any others' work, paragraphs, text, data, results, etc., reported in journals, books, magazines, reports dissertations, theses, etc., or available at websites and have not included them in this thesis and have not cited as my own work.

Date: 27.12.24


  
Signature of the Student


Place: IIT (BHU), Varanasi

(Nidhi Goel)

## Certificate by the Supervisor

It is certified that the above statement made by the student is correct to the best of my knowledge.

  
Signature: Supervisor  
**Assistant Professor** (Somnath Nag)  
**Department of Physics**  
**Indian Institute of Technology**  
**(Banaras Hindu University)**  
**Varanasi-221005**

  
Signature of the Head of the Department  
(Prof. Sandip Chatterjee)  
**HEAD/विभागाध्यक्ष**  
**भौतिकी विभाग/Deptt. of Physics**  
**मा0प्रौ0सं0/(का0हि0वि0)/IIT (BHU)**  
**वाराणसी/Varanasi-221005**



## Copyright Transfer Certificate


**Title of the Thesis :** Study of evolution of energetically favored collectivity and hindered isomeric states in the  $A \approx 90$  region

**Name of the Student :** Nidhi Goel

### Copyright Transfer

The undersigned hereby assigns to the Indian Institute of Technology (Banaras Hindu University) Varanasi all rights under copyright that may exist in and for the above thesis submitted for the award of the **Doctor of Philosophy in Physics**.

Date: 27.12.24

  
Signature of the Student

Place: IIT (BHU), Varanasi

(Nidhi Goel)

**Note: However, the author may reproduce or authorize others to reproduce material extracted verbatim from the thesis or derivative of the thesis for author's personal use provided that the source and the Institute's copyright notice are indicated.**

## Acknowledgements

The idea of a societal coexistence solely depends on conscious and purposeful cooperation from each and every wing of society. In turn, it owes to us that we acknowledge the help and support we receive during each step in life. However, it may not be possible to pen down the words of gratitude in a few paragraphs. Even if I miss to address any name, I would remain indebted to all those who stood by throughout my journey to a PhD.

A PhD thesis in the field of experimental nuclear structure cannot be completed without the immense support of academic and non-academic members in academia. I am grateful to my PhD supervisor, Dr. Somnath Nag, for his continuous guidance and sincere advice throughout the thesis work. During the course of my thesis-writing process, he facilitated invaluable discussions and generated numerous beneficial ideas. I am thankful to him for his clear and enthusiastic discussions and suggestions, which helped me to find my firm grounding in the research problem. Without his dedicated supervision, completing this thesis would have never been possible. I am thankful to the RPEC members, Dr. Somak Bhattacharyya and Dr. Gauhar Abbas, for their constructive suggestions during this journey. I would remain obliged to the Department of Physics, IIT(BHU). I remain grateful to the HODs of the department, Prof. Prabhakar Singh, and Prof. S. Chatterjee. Further, I would remain indebted to all the faculty members of the department. The non-teaching members of the institute also deserve a special mention, who helped in conducting all the required administrative work smoothly.

Sincere acknowledgement is due for the financial assistance received from the MoE and IIT(BHU) during the tenure. The funding to my supervisor from SERB-DST (ANRF) under contract no. CRG/2021/006671 is also acknowledged.

I would like to express my gratitude to Prof. R. Palit for his immense support with the experimental data and the analysis. I am also grateful to Prof. A. K. Singh and Prof. I. Ragnarsson for their constant guidance in data analysis and model calculations. All

the other collaborators, including Dr. D. Choudhury, Dr. P.C. Srivastava, and Dr. B. Maheshwari, deserve a special mention. The experiments would not have been successful without the sincere support of the operation staff and target lab personnel at TIFR.

All through the PhD work, I really enjoyed the company of my colleagues, Mamta Prajapati and Aalakh Kumar and also the master's degree project scholars. During various outstation stays for academic purposes, I shared fruitful moments with Dr. Sutanu Bhattacharya, Dr. Piku Dey, Dr. Ananya Kundu, Dr. Biswajit Das, Vishal Malik, Sahab Singh, Rajat, Atreyee Dey, Gourchand Manna and Rupesh Kumar.

Friends at various stages of my career would remain special to me. A thank you word is not enough to express my gratitude towards my dearest friend Manisha, Kartika, Samiksha, Vindya, Ashish Kumar Singh and Aman Grover for just being there in my happiness and sorrow.

A long journey like a PhD amid the ups and lows in life can never be converted to a successful endeavour without the support, love and "Ashirvaad" of near and dear ones in one's family. I may fall short of Words to express my gratitude towards my Amma, parents, brothers and sisters, my chacha and chachi and my in-laws. They extended their emotional support, and their encouragement will always keep on inspiring me throughout my entire life. Finally, the love of my life, my husband, Mr. Vinayak Pundir, deserves special recognition for his love, care and support. I am grateful for his patience in listening to all my academic and non-academic conversations.

These past years have been a transformative journey for me. The vibrant atmosphere of this beautiful green campus has contributed immensely to my overall experience. In the end, I thank Almighty God for everything.

—

**Nidhi Goel**

---

## List of Acronyms

---

Acronym	Full form
ADC	Analog to Digital Converter
ACQ	Acquisition
BGO	Bismuth Germanate
CFD	Constant Fraction Discriminator
CNS	Cranked Nilsson Strutinsky
CU	Coincidence Unit
DCO	Directional Correlation
DDAQ	Digital Data Acquisition
FADC	Flash Analog to Digital Converter
FET	Field Effect Transistor
FIFO	Fast-In Fast-Out
FWHM	Full Width at Half Maximum
HPGe	High-Purity Germanium
INGA	Indian National Gamma Array
IPDCO	Integrated Polarization-Directional Correlation
LD	Liquid Drop
LDM	Liquid Drop Model
LSD	Lublin-Strasbourg Drop
LVDS	Low Voltage Differential Signalling
MARCOS	Multi Parameter Time-Stamp-Based Coincidence Search Program
PDCO	Polarization-Directional Correlation
PES	Potential Energy Surface
PT	Peak to Total
RLD	Rotating Liquid Drop
TFA	Timing Filtering Amplifier
TIFR	Tata Institute of Fundamental Research

---

---

## List of Symbols

---

Symbols	Definition (unit)
$A$	Mass number
$\alpha$	Signature quantum number
$\beta$	Axial deformation parameter
$\Delta$	Pairing gap energy
$\Delta_{asym}$	Polarization asymmetry parameter
$\varepsilon_2$	Quadrupole deformation parameter
$e_i$	Single-particle energy in MeV
$E$	Energy in proper units
$E2$	Electric quadrupole transition
$\gamma$	Triaxiality deformation parameter
$\hbar$	Reduced Plank constant ( $m^2kg/s$ )
$\mathcal{H}$	Hamiltonian
$I$	Total angular momentum of the nucleus
$i_x$	Aligned angular momentum in units of $\hbar$
$j$	Total angular momentum of nucleons; $j = l + s$
$j_x$	Projection of total angular momentum of on x axis
$J$	Moment of inertia of the system
$J_{rig}$	Rigid body moment of inertia
$J^{(1)}$	Kinematic moment of inertia of the system ( $\hbar/MeV$ )
$J^{(2)}$	Dynamic moment of inertia of the system ( $\hbar^2/MeV$ )
$l$	Orbital angular momentum
$\lambda$	Multipole mode
$\Lambda$	Projection of orbital quantum number along the symmetry axis
$m/M$	Mass
$\mu$	Reduced mass
$m_o$	Rest mass of the electron
$M1$	Magnetic dipole transition

---

<b>Symbols</b>	<b>Definition (unit)</b>
$N$	Neutron number
$N_q$	Principal quantum number
$\omega$	angular frequency
$\Omega$	The projection of angular momentum along the symmetry axis
$R$	Radius in appropriate units
$R_\theta$	Angular distribution ratio
$s$	Spin angular momentum
$\Sigma$	Projection of spin quantum number along the symmetry axis
$\theta$	Angle
$V$	Potential in appropriate units
$Y_{20}(\theta, \phi)$	Spherical polar harmonics
$Z$	Proton number

---

# List of Figures

1.1	Schematic diagram of the shape parameters in rotating quadrupole deformed nuclei . . . . .	2
1.2	Examples of angular momentum generation through single-particle excitations at lower excitation energy and through collective excitations at higher excitation energy in nearly-spherical $^{90}\text{Y}$ . This is the near yrast level scheme for $^{90}\text{Y}$ , reproduced from reference. . . . .	4
1.3	Single-particle levels in the $^{208}\text{Pb}$ , $^{146}\text{Gd}$ region and in the $^{90}\text{Zr}$ region. The single-particle energies are given with respect to an arbitrary zero point. . . . .	5
1.4	Experimental systematics of isomers in $N = 51$ isotones . . . . .	9
1.5	The characteristic diagram of $B(M1)$ values with spin $I$ for the magnetic rotational bands in $^{89}\text{Zr}$ and $^{90}\text{Y}$ nuclei . . . . .	11
1.6	Calculated total energy surfaces with pairing included for the $(\pi, \alpha)_p$ $(\pi, \alpha)_n = (+, 0)_p$ $(+, 0)_n$ combination of quantum numbers at $I = 10, 20$ , and $26\hbar$ . At each point, the total energy has been minimized with respect to $\epsilon_4$ , $\lambda_{p,n}$ and $\Delta_{p,n}$ as well as quasiparticle configuration. The contour line separation is 0.25 MeV. The figure is drawn for $\gamma = -120^\circ, 60^\circ$ with the $\gamma = 0^\circ$ and $-60^\circ$ axes labeled in the $I = 26$ surface in $^{142}\text{Gd}$ . . . . .	13
1.7	Partial (high-spin) level scheme of (a) $^{142}\text{Gd}$ (b) $^{89}\text{Zr}$ . . . . .	14

1.8	Calculated total energy surface plot for $^{89}\text{Zr}$ . The contour line separation is 0.25 MeV. . . . .	15
1.9	Panel (a) dipole bands of $^{89}\text{Y}$ and Panel (b) dipole bands of $^{90}\text{Zr}$ . . . . .	16
1.10	Excitation energies relative to rotating-liquid drop energy, for observed (upper panel) and calculated (lower panel) valence-space states for $^{89}\text{Y}$ . Difference between the observed and calculated results have been shown in the third panel. . . . .	17
1.11	Calculated total energy surfaces plots for positive parity (band 1) spin of $13.5\hbar$ , $15.5\hbar$ , $18.5\hbar$ and $20.5\hbar$ for $[43;11] \pi((fp)^{-4}(g_{9/2})^3 \otimes \nu(g_{9/2})^{-1}(gd)^1)$ in $^{89}\text{Y}$ . The contour line separation is 0.25 MeV. . . . .	18
1.12	Total energy surfaces for band 2, the configuration $[32;22] \pi((fp)^{-3}g_{9/2}^2) \otimes \nu(g_{9/2}^{-2}(gd)^2)$ for spins $13.5\hbar$ to $21.5\hbar$ in $^{89}\text{Y}$ . The contour line separation is 0.25 MeV. . . . .	19
1.13	Calculated total energy surfaces plots for positive parity spin of $16\hbar$ , $17\hbar$ , $18\hbar$ and $19\hbar$ for general scan in $^{90}\text{Nb}$ . The contour line separation is 0.25 MeV. . . . .	20
1.14	Excitation energies relative to rotating-liquid drop energy, for observed (upper panel) and calculated (lower panel) valence-space states for $^{90}\text{Zr}$ . Difference between the observed and calculated results have been shown in the third panel. . . . .	22
1.15	Calculated total energy surfaces plots for positive parity spin of $14\hbar$ , $16\hbar$ , $18\hbar$ and $20\hbar$ for $[33;11] \pi((fp)^{-3}g_{9/2}^3) \otimes \nu(g_{9/2}^{-1}(gd)^1)$ in $^{90}\text{Zr}$ . The contour line separation is 0.25 MeV. . . . .	23
1.16	Calculated total energy surfaces plots for positive parity spin of $13.5\hbar$ , $15.5\hbar$ , $17.5\hbar$ and $19.5\hbar$ for general scan in $^{91}\text{Zr}$ . The contour line separation is 0.25 MeV . . . . .	24

---

2.1	Schematic diagram illustrating the various modes of formation and decay of a compound nucleus. The Figure taken from Ref. [1] . . . . .	29
2.2	Schematic illustration of high spin residual nuclear isotope from decay of compound nucleus. The Figure taken from Ref. [1] . . . . .	30
2.3	Schematic diagram of HPGe detector with Compton suppression shield. .	35
2.4	The left panel shows a single HPGe crystal, whereas the rightmost panel displays a closely packed arrangement of four crystals that form a clover. .	36
2.5	INGA set up at T.I.F.R. Mumbai. . . . .	38
2.6	Block diagram of Pixie-16 module. . . . .	40
2.7	Relative efficiency curve vs energy of transition for all detectors of INGA set up. . . . .	43
2.8	Angular distribution for a dipole transition in $^{92}\text{Nb}$ with a energy of transition 322.2 keV. . . . .	46
2.9	The asymmetry factor as a function of $\gamma$ -ray energies for INGA set up at TIFR. . . . .	48
2.10	Schematic diagram shows the experimental lineshape of a transition decaying from a state whose level lifetime $\sim 1$ ps. The resulting $\gamma$ -ray Doppler shift as observed by the detectors placed at (a) a backwards angle ( $\theta$ ) close to $90^\circ$ , (b) a backwards angle $\theta$ , $180^\circ > \theta > 90^\circ$ , (c) an forward angle $\theta$ , $90^\circ > \theta > 0^\circ$ , and (d) forward angle $\theta = 0^\circ$ . . . . .	49
2.11	Construction of the time difference spectrum between two $\gamma$ rays feeding (2211.0-keV) and de-exciting (115.4-keV) through the state of interest ( $11^-$ ). .	52

- 2.12 The time-difference spectra were constructed from the present data on  $^{92}\text{Nb}$  using the 2211.0-keV transition as a “start” and the 115.4-keV transition below the isomeric level as “stop”. The solid red line, showing the fitting to the selected portion of the experimental spectrum by fitting a convoluted Gaussian and exponential function to the time difference spectrum, gives a half-life of 103.6(32)ns. The prompt was constructed with the coincidence of 327.7 and 2286.6 keV transitions as “start” and “stop”, respectively. The prompt curve is fitted with the Gaussian function and is displayed by the blue color solid line. The blue Gaussian curve is used as a representative plot to compare the shape of the time spectrum between the prompt and the delayed peak. The prompt curve y-axis is scaled down by a factor of  $\sim 6$ . The prompt curve has not been used to fix the Gaussian width of the fits across the delayed curve. It is hereby mentioned that the data points from -120 ns to -200 ns have been considered for the fitting of the delayed curve. 54
- 3.1 Single particle energy levels for square-well potential alongwith the inclusion of anharmonic term as well as spin orbit coupling. . . . . 58
- 3.2 Nilsson diagram showing proton and neutron single-particle energies with the shell closure (a)  $28 < Z < 50$  (b)  $50 < N < 82$  as a function of deformation parameter  $\epsilon_2$ . . . . . 63
- 3.3 Rotating body-fixed coordinate system (shown with primed coordinates) with respect to laboratory frame of reference. . . . . 67
- 3.4 Single-particle energies as a function of spin projection for rotation around symmetry axis. . . . . 69

- 3.5 Single particle Routhians for protons typical triaxial deformation parameters  $\varepsilon_2 = 0.15$ ,  $\gamma = 30^\circ$  and  $\varepsilon_4 = 0.004$ . Four combinations of different  $(\pi, \alpha)$  are plotted with the following representation: solid lines are for (+, +1/2), dotted lines represent (+, -1/2) whereas (-, +1/2) and (-, -1/2) are shown by dashed and dashed-dotted lines respectively. The labeling of the orbitals is done for zero rotational frequency.  $fp$  and  $gd$  represent the orbitals with dominant amplitudes in and  $(p_{1/2}, p_{3/2}, f_{5/2})$   $(g_{7/2}, d_{5/2})$  respectively with the ordering and  $\Omega$ -values as subscripts. The black thick arrow signifies the position of the Fermi level. For clarity, the number of nucleons are mentioned at the zero rotational frequency. . . . . 75
- 4.1 Partial level scheme of  $^{92}\text{Nb}$ . The  $9^-$  and  $11^-$  isomers were assigned with the measured half-lives, 35.8(23) ns and 103.6(32) ns, respectively, in this work. The newly measured half-life of  $11^-$  isomer is shorter than the previous measurement 167(4) ns which has been reported by Brown *et al.* The details of the intensity of  $\gamma$  transitions, branching ratios, and conversion coefficients are given in Table. The thickness of the arrows across each transition measures its relative intensity with respect to 327.7-keV  $\gamma$  ray, whose intensity has been normalized to 100. To include the effect of isomeric half-lives on the intensity distribution of the corresponding transitions, a longer time window of 400 ns was considered. . . . . 80

- 4.2 The  $\gamma$ - $\gamma$  coincidence spectrum gated on (panel (a)) 2087.3- and (panel (b)) 327.7-keV transitions within a time window of 200 ns. The transitions marked with black labels correspond to the ones considered in the present study of  $^{92}\text{Nb}$  whereas the ones shown with blue colored labels belong to  $^{92}\text{Nb}$  but are not within the scope of the present analysis. The contaminant peaks from  $^{92}\text{Mo}$  are shown in red color. . . . . 82
- 4.3 A plot of excitation energy versus spin for states in  $^{91}\text{Nb}$  and  $^{92}\text{Nb}$  are indicated by closed and opened circles, respectively. Squares indicate the isomeric states. . . . . 82
- 4.4 The time-difference spectra were constructed using (a) the 147.6-keV transition as a “start” and the 2087.3-keV transition below the isomeric level as “stop”, and (b) the 115.4-keV transition as a “start” and the 2087.3-keV transition as “stop”. The solid red line, showing the fitting to the selected portion of the experimental spectrum by fitting a convoluted Gaussian and exponential function to the time difference spectrum, gives a half-life of 34.0(12)ns (panel a) and 38.8(16) ns (panel b). The prompt was constructed with the coincidence of 327.7 and 2286.6-keV transitions as “start” and “stop” respectively. The prompt curve is fitted with the Gaussian function and is displayed by the blue color solid line. The blue Gaussian curve is used as a representative plot to compare the shape of the time spectrum between the prompt and the delayed peak. The prompt curve y-axis is scaled up by a factor of  $\sim 2$  and  $\sim 1.3$  in Fig. 4.4(a) and 4.4(b) respectively. The prompt curve has not been used to fix the Gaussian width of the fits across the delayed curve. It is hereby mentioned that the data points from -150 ns to -200 ns have been considered for the fitting of the delayed curve. . . . . 83

- 
- 4.5 Comparison of experimental levels and shell model calculated levels for odd-A nuclei  $^{91}\text{Nb}$  using Set1 and Set2. . . . . 87
- 4.6 Comparison of experimental levels and shell model calculated levels of nucleus  $^{92}\text{Nb}$  using Set1 and Set2. . . . . 87
- 5.1 The partial level scheme of  $^{93}\text{Nb}$ . Newly observed gamma transitions are marked by an asterisk and labelled in red color while rearranged transitions are indicated in blue. The thickness of the arrow represents the relative intensity of the gamma rays as mentioned in Table A.4. . . . . 97
- 5.2  $\gamma\text{-}\gamma$  coincidence spectrum gated on 949.5-keV transition. Transitions (in red color) marked with \* are newly observed ones. The peak with parentheses in green color is contamination. . . . . 98
- 5.3 The  $\gamma\text{-}\gamma$  coincidence spectrum gated on 759.2-keV transition. Transitions in red color marked with \* are newly observed ones. Peaks with parentheses in green color are contaminated peaks from nuclei  $^{92}\text{Nb}$ . . . . 99
- 5.4 The  $\gamma\text{-}\gamma$  coincidence spectrum gated on 1039.1-keV transition. Transitions in red color marked with \* are newly observed, and those in blue are shuffled to the new positions. . . . . 100
- 5.5 The  $\gamma\text{-}\gamma$  coincidence spectrum gated on (a) 1039.1- , (b) 1271.3- , and (c) 1496.9-keV transitions. Transitions in red color marked with \* are newly observed ones. . . . . 101
- 5.6  $\gamma\text{-}\gamma$  coincidence spectrum gated on 1496.9- and 1530.2-keV transition. Transitions in red color marked with \* are newly observed, and those in blue are displaced. Peaks with parentheses in green color are contamination. 102

- 5.7 The time-difference spectra were constructed using the 392.8-, 496.4-, 1699.1- and 941.4-keV transitions as a “start” and the 1530.2-, 392.8-, 1530.2-, and 1530.2-keV transitions as “stop” shown in panels a, b, c, and d respectively. . . . . 103
- 5.8 Representative spectra along with theoretically fitted lineshapes for (a) 1039.1.7 keV, (b) 1271.3 keV, (c) 1496.9 keV and (d) 1530.2 keV quadrupole transitions in quadrupole ground state band of  $^{93}\text{Nb}$ . The top, middle, and bottom rows correspond to the shapes in the  $157^\circ$ ,  $90^\circ$ , and  $65^\circ$  detectors, respectively. The desired lineshapes of gamma transitions, contaminant peaks, and total lineshapes are represented by the blue, green, and red curves, respectively. . . . . 104
- 5.9 Representative spectra along with theoretically fitted lineshapes for (a) 392.8 keV, (b) 614.6 keV, (c) 496.4 and (d) 485.5 keV dipole transitions in the dipole band of  $^{93}\text{Nb}$ . The upper and lower rows correspond to the shapes in the  $140^\circ$  and  $90^\circ$  detectors, respectively. The blue, green, and red curves represent the desired lineshapes of gamma transitions, contaminant peaks, and total lineshapes. . . . . 105
- 5.10 Excitation energies relative to rotating-liquid drop energy as a function of angular momentum, for observed ( panel a) and calculated (panel b) valence-space states for  $^{93}\text{Nb}$ . The difference between the observed and calculated results has been shown in panel c. The closed and the open circles represent the ( $\alpha = +1/2$ ) and the ( $\alpha = -1/2$ ) states respectively. The positive parity configuration is shown by solid lines whereas the configurations with negative parity are drawn with broken lines. Aligned states are encircled. . . . . 109

- 5.11 Calculated total energy surfaces for spin  $6.5\hbar$  to  $16.5\hbar$  [23;02] ground band configuration for band A in  $^{93}\text{Nb}$ . The contour line separation is 0.25 MeV. . . . . 110
- 5.12 Calculated sloping Fermi-surface plots. Representing the maximum spin state in [23<sub>+</sub>;02], configuration in  $^{93}\text{Nb}$ . . . . . 111
- 5.13 Calculated total energy surfaces for  $18.5\hbar$ ,  $19.5\hbar$ ,  $20.5\hbar$  and  $22.5\hbar$  for [23;121] band 1 in  $^{93}\text{Nb}$ . . . . . 114
- 5.14 Single particle Routhians for protons (a) and neutrons (b) typical triaxial deformation parameters  $\varepsilon_2 = 0.15$ ,  $\gamma = 30^\circ$  and  $\varepsilon_4 = 0.004$ . Four combinations of different  $(\pi, \alpha)$  are plotted with the following representation: solid lines are for  $(+, +1/2)$ , dotted lines represent  $(+, -1/2)$  whereas  $(-, +1/2)$  and  $(-, -1/2)$  are shown by dashed and dashed-dotted lines respectively. The labelling of the orbitals is done for zero rotational frequency.  $[fp]$  and  $[gd]$  represent the orbitals with dominant amplitudes in and  $(p_{1/2}, p_{3/2}, f_{5/2})$   $(g_{7/2}, d_{5/2})$  respectively with the ordering and  $\Omega$ -values as subscripts. The black thick arrow signifies the position of the Fermi level. For clarity, the number of nucleons are mentioned at the zero rotational frequency. . . . . 115
- 5.15 ( Calculated total energy surfaces for  $8.5\hbar$ ,  $10.5\hbar$   $12.5\hbar$  for [12;02] and  $14.5\hbar$  for [23;011] band 1 configuration in  $^{93}\text{Nb}$ . . . . . 117
- 6.1 The level scheme of  $^{92}\text{Nb}$ . Newly observed gamma transitions are marked by red labels, while rearranged transitions are indicated in blue. The thickness of the arrow represents the relative intensity of the gamma rays as mentioned in A.5. . . . . 122

6.2	$\gamma$ - $\gamma$ coincidence spectrum gated on 2087.3-keV transition. Transitions marked with * are newly observed ones. Transitions constituting band 1 and band 2 have been shown in the spectrum. The peak with parentheses is contamination. . . . .	124
6.3	$\gamma$ - $\gamma$ coincidence spectrum gated on 327.7-keV transition. Transitions marked with * are newly observed ones. Peaks with parentheses are contamination. . . . .	125
6.6	$\gamma$ - $\gamma$ coincidence spectra gated on (a) 1256.3- and (b) 1331.0-keV transitions. Transitions marked with * are newly observed ones. Transition marked with # has been placed by Zheng <i>et al.</i> which were not observed in the present work. The present study provides clear evidence for the absence of a 674.8 keV in the 1256.3 keV gate and 549.9-,580.2-,610.1-, and 718.7 keV in the gate 1331.0 keV transition. Peaks with parentheses are contamination. . . . .	126
6.9	Representative spectra along with theoretically fitted lineshapes for (a) 1550.3 keV, (b) 610.1 keV, (c) 580.2 keV, (d) 674.8 keV, (e) 513.4 keV and (f) 718.7 keV dipole transitions in the dipole band of $^{92}\text{Nb}$ . The upper, middle and lower rows correspond to the shapes in the $140^\circ$ , $90^\circ$ and $65^\circ$ detectors, respectively. The blue, green, and red curves represent the desired lineshapes of gamma transitions, contaminant peaks, and total lineshapes. . . . .	131
6.10	Total energy surfaces for general scan run for a spin $14\hbar$ to $21\hbar$ in $^{92}\text{Nb}$ . The contour line separation is 0.25 MeV. . . . .	137
6.13	Calculated total energy surfaces for $14\hbar$ , $17\hbar$ , $18\hbar$ , $19\hbar$ , $20\hbar$ , $21\hbar$ for [34;12] in $^{92}\text{Nb}$ . . . . .	141

# List of Tables

4.2	The calculated $B(E2)$ results are listed for both Set1 and Set2 as described in the text. . . . .	90
5.1	Measured lifetimes of states in the band A consisting of quadrupole transitions, $\tau$ (ps), and corresponding reduced transition strengths. Systematic errors due to uncertainties in the stopping powers used are not included. . . . .	105
5.2	Measured lifetimes of states in the $M1$ band, $\tau$ (ps), and corresponding $B(M1) \mu_N^2$ reduced transition strengths. Systematic errors due to uncertainties in the stopping powers used are not included. . . . .	106
6.1	Measured lifetimes of states in the $M1$ band, $\tau$ (ps), and corresponding $B(M1) \mu_N^2$ reduced transition strengths. Systematic errors due to uncertainties in the stopping powers used are not included. . . . .	133
A.1	Energies, intensities, branching ratio, internal conversion coefficients, spin and multipolarities assignments of $\gamma$ -ray transitions of $^{92}\text{Nb}$ . . . . .	165

- A.2 The average occupancies of active orbitals for various spin states in set 1 shell model calculations of  $^{92}\text{Nb}$ . The columns  $\langle L_p \rangle$  and  $\langle L_n \rangle$  list the expectation of orbital angular momentum contributions from the proton and neutron sides, respectively. The  $l_s$  value (just below orbital) indicates the nature of the orbital, where  $l$  denotes the orbital angular momentum as 0,1,2,3,4..., and  $s$  as a suffix signifies the spin angular momentum, with '+' and '-' denoting  $+1/2$  and  $-1/2$  values, respectively. . . . . 166
- A.3 The average occupancies of active orbitals for various spin states in set 2 shell model calculations of  $^{92}\text{Nb}$ . The columns  $\langle L_p \rangle$  and  $\langle L_n \rangle$  list the expectation of orbital angular momentum contributions from the proton and neutron sides, respectively. The  $l_s$  value (just below orbital) indicates the nature of the orbital, where  $l$  denotes the orbital angular momentum as 0,1,2,3,4..., and  $s$  as a suffix signifies the spin angular momentum, with '+' and '-' denoting  $+1/2$  and  $-1/2$  values, respectively. . . . . 167
- A.4 Energies, intensities, angular distribution ratios, multipolarities and spin assignments of  $\gamma$ -ray transitions of  $^{93}\text{Nb}$ . The experimentally observed values are given for  $\gamma$  transition energy whereas the level energies are the output of the Gamma-to-Level (GTOL) least-squares fitting code developed at NNDC . . . . . 168
- A.5 Energies, intensities, angular distribution ratios, multipolarities and spin assignments of  $\gamma$ -ray transitions of  $^{92}\text{Nb}$ . The experimentally observed values are given for  $\gamma$  transition energy whereas the level energies are the output of the Gamma-to-Level (GTOL) least-squares fitting code developed at NNDC . . . . . 169
- A.6 The calculated shell model wave functions corresponding to different energy states in  $^{92}\text{Nb}$ . . . . . 173